Kumar *et al.*
Future Journal of Pharmaceutical Sciences (2024) 10:18
https://doi.org/10.1186/s43094-024-00588-3

Future Journal of Pharmaceutical Sciences

RESEARCH

Open Access

Development of superior chitosan–EDTA microparticles as an adsorbent base for solidifying the self-emulsifying drug delivery systems

Mohit Kumar[1], Pooja A. Chawla[2*], Abdul Faruk[1*], Viney Chawla[2*], Shubham Thakur[3] and Subheet Kumar Jain[4]

Abstract

Background The present study focused on developing a superior adsorbent carrier (microparticles) to solidify the self-emulsifying drug delivery system. The two approaches, solvent evaporation and spray drying, were explored to synthesize the microparticles using chitosan (CH) and EDTA disodium. The 3^2 full factorial design was applied to optimize the microparticle process produced by both methods.

Results The various characterization evaluations of the microparticles revealed amide linkages between the CH and EDTA disodium, and XRD results showed that microparticles were amorphous. The SE-CHEM (C_2) and SD-CHEM (Y_1) optimized microparticles were free-flowing and had percentage yield (%), 96 ± 1.2 and 58 ± 1.1, zeta potential (mV), 9 ± 0.44 and 4 ± 0.13, and particle size (μm), 3 ± 0.57 and 2 ± 0.4, respectively. SEM images showed uneven surfaces with wide void spaces and flaky texture for optimized microparticles Y_1 and C_2, respectively. The SE-CHEM (C_2) had an oil adsorption capacity (OAC %) of 46 ± 0.54 and 60 ± 0.77, and oil desorption capacity (ODC %), 38 ± 0.65 and 56 ± 0.86, for Labrafac and Cremophor RH 40, respectively. The SD-CHEM (Y_1) had an oil adsorption capacity (OAC %) of 59 ± 0.71 and 68 ± 0.39, and oil desorption capacity (ODC %), 54 ± 0.11 and 65 ± 0.74, for Labrafac and Cremophor RH 40, respectively. In the surface free energy components analysis, the SE-CHEM (C_2) had an enhanced dispersive component [γ^{LW} (mJ/m^2)] of 32 ± 0.68 and 37 ± 0.47 for Labrafac and Cremophor RH 40, respectively. The SD-CHEM (Y_1) had an enhanced dispersive component [γ^{LW} (mJ/m^2)] of 48 ± 0.7 and 52 ± 0.41 for Labrafac and Cremophor RH 40, respectively. The SE-CHEM (C_2) had enhanced dynamic advancing contact angles [θ_a (°)] of 75 ± 0.19 and 78 ± 0.75 for Labrafac and Cremophor RH 40, respectively. The SD-CHEM (Y_1) had enhanced dynamic advancing contact angles [θ_a (°)] of 74 ± 0.6 and 80 ± 0.21 for Labrafac and Cremophor RH 40, respectively.

Conclusion All the findings indicate that the microparticles have superior characteristics to serve as the adsorbent base for solid self-emulsifying drug delivery systems.

Keywords Adsorbent carriers, Solid self-emulsifying drug delivery systems, Solvent evaporation, Spray drying, Microparticles, Optimization, Surface free energy components

*Correspondence:
Pooja A. Chawla
pvchawla@gmail.com
Abdul Faruk
abdul_faruk@yahoo.com
Viney Chawla
drvineychawla@gmail.com
Full list of author information is available at the end of the article

Background

Solid self-emulsifying drug delivery systems (S-SEDDS) are well-proven and known formulation systems. They offer many advantages like increased surface area (which offers high solubility and bioavailability), robustness, high stability, high scalability, ease in handling, high drug loading, better flowability, decreased drug precipitation and economical production [1]. S-SEDDS can be turned into Self-emulsifying pellets and tablets, which are far more stable than SEDDS and S-SEDDS powder [2, 3]. Despite the excellent advantages of S-SEDDS, problems like liquid squeezing out, low disintegration, inadequate hardness and compaction issues are observed. Because of physicochemical interactions between the solid carrier, oil base and surface-active agents, limited release of the formulation can be a problem [4]. Therefore, a suitable adsorbent carrier becomes the most vital part of the stability of the S-SEDDS [5]. Different carriers like PVP K-30, maltodextrin, magnesium stearate, β-cyclodextrin, polyvinyl alcohol, neusilin US2, sodium CMC, dextrin, lactose, mannitol, HP-β-CD, aerosil-200, syloid 244FP, avicel PH102, syloid XDP 3150 and microcrystalline cellulose are used [6].

An ideal solid adsorbent carrier must have high oil adsorption and desorption capacity, wide interparticle void space and low porosity [7]. Usually, hydrophobic carriers have high OAC (oil adsorption capacity) and high flowability [8]. A solid carrier with high OAC is required less in amount, resulting in a lower dosage form [7, 8]. Formulations high in surfactant concentration adsorb well on hydrophobic adsorbents [9]. A high concentration of surfactants forms very small-sized droplets. Hence, an attempt was made to prepare such solid adsorbent carriers (microparticles) of chitosan with EDTA disodium by solvent evaporation and spray drying. Chitosan produces a clear solution with EDTA disodium in acetic acid [10]. This solution was subjected to solvent evaporation and spray drying to produce microparticles, which should be hydrophobic to ensure that the surface of these particles can be used for drug adsorption in the lipid phase [11]. The amide linkages in microparticles form a hydrophobic interpenetrating rough surface [12]. So, the present study aims to optimize microparticles by 3^2 full factorial experimental designs for solvent evaporation and spray drying methods. The chitosan–EDTA microparticles (CHEM) were characterized for their suitable hydrophobic surface to act as a good adsorbent base for S-SEDDS.

Materials and methods

Chitosan 90% DA (deacylated) was purchased from Marine hydrocolloids (Kerala, India). Ethylenediaminetetraacetic acid disodium (EDTA disodium) was purchased from CDH (India). Other chemicals purchased were Acetic acid (Rankem RFCL, India) and diiodomethane (TCI, Japan). Cremophor RH 40 (Himedia, India). Labrafac™ PG was a gift from Gattefossé (Canada). Other chemicals used were of analytical grade. They were used as received.

Design of experiment

To optimize the preparation of blank microparticles (CHEM), 3^2 full factorial design was used. The concentration ratio of chitosan–EDTA disodium and drying temperatures were observed as the critical factors and were two independent variables. Both had three different levels. Factors like zeta potential, percentage yield and particle size were considered dependent variables. All the responses were fitted in the least fit squares regression analysis using JMP 16 (Trial). Various outcomes of the mathematical model, like the actual vs predicted plot, ANOVA analysis, parameter estimates, model equation, prediction profiler, response surface, contour profilers, Pareto charts and optimization desirability, were determined to validate the model [13]. The desirability function was used for the selected responses for the optimization process. So, Y (practical yield, %) had to be maximized, ZP (zeta potential, mV) had to be maximized, and PS (Particle size, μm) had to be minimized.

The overall percentage of chitosan–EDTA disodium in solution was kept at 2% w/v because its viscosity remains adequate for flow at this concentration. Further, as mentioned in Table 1, three different ratios of chitosan–EDTA disodium (40:60, 50:50 and 60:40) were prepared.

Firstly, a weighed amount of chitosan was taken in a beaker and dissolved in 1 M (5.72%) glacial acetic acid at 800 rpm in a magnetic stirrer for two hours. A separate solution of EDTA disodium with double distilled water was prepared. EDTA disodium solution was added dropwise to chitosan solution under continuous vigorous stirring over 2000 rpm with a mechanical stirrer for 25–30 min to get a clear ionic solution [14]. Further, these different solutions were subjected to solvent evaporation and spray drying using a 3^2 full factorial design.

Preparation of Chitosan–EDTA microparticles (SE-CHEM) by solvent evaporation method

All three ratios of chitosan–EDTA disodium solutions were subjected to solvent evaporation in a Rota

Table 1 3^2 Full factorial design for SE-CHEM

Codes	CH (ratio)	Level codes	DT (°C)	Level codes	Y (%)	ZP (mV)	PS (μm)
A_1	40:60	1	50	1	79 ± 1.3	0.39 ± 0.13	27 ± 2.1
A_2	40:60		70	2	81 ± 0.8	0.43 ± 0.11	16 ± 1.7
A_3	40:60		90	3	87 ± 1.1	0.51 ± 0.16	15 ± 1.1
B_1	50:50	2	50	1	88 ± 0.4	3.00 ± 0.11	14 ± 0.4
B_2	50:50		70	2	90 ± 0.5	3.00 ± 0.24	11 ± 0.17
B_3	50:50		90	3	91 ± 0.4	4.00 ± 0.45	6 ± 0.9
C_1	60:40	3	50	1	93 ± 0.9	5.00 ± 0.35	4 ± 0.84
C_2	60:40		70	2	96 ± 1.2	9.00 ± 0.44	3 ± 0.57
C_3	60:40		90	3	94 ± 0.8	5.00 ± 0.85	5 ± 0.78

*CH-CH:EDTA ratio, DT-drying temp., Y-percentage yield, ZP-zeta potential, PS-particle size

Table 2 3^2 Full factorial design for SD-CHEM (mention full form of this formulation)

Codes	CH (ratio)	Level codes	DT (°C)	Level codes	Y (%)	ZP (mV)	PS (μm)
X_1	40:60	− 1	110	1	26 ± 0.8	− 3 ± 0.45	5 ± 1.4
X_2	40:60		130	2	30 ± 1.2	− 3 ± 0.24	4 ± 0.8
X_3	40:60		150	3	37 ± 0.6	2 ± 0.8	4 ± 0.6
Y_1	50:50	1	110	1	58 ± 1.1	4 ± 0.13	2 ± 0.4
Y_2	50:50		130	2	44 ± 0.9	2 ± 0.5	2 ± 0.9
Y_3	50:50		150	3	25 ± 0.7	1 ± 0.7	3 ± 1.1

*CH-CH:EDTA ratio, DT-drying temp., Y-percentage yield, ZP-zeta potential, PS-particle size

vacuum evaporator (Micro technologies, India) at a drying temperature range from 50 to 90 °C for 45–60 min, as in Table 2. Then, the dry film was scrapped carefully and dried in an oven to remove residual moisture for 40–50 min at 70 °C. The dried film was converted into powder by using a pestle mortar.

Preparation of Chitosan–EDTA (SD-CHEM) microparticles by spray drying

The following overall spray drying specifications were used: Inlet temperature 110–150 °C, outlet temperature 50–70 °C, aspirator speed 1000–2000 rpm, atomization pressure 3 kg/cm^2 and feed pump at 15 rpm in Spray dryer (SprayMate JISL, India). The two ratios of solutions (40:60 and 50:50) were easily spray-dried. It was observed that the high chitosan ratio solution (60:40) posed a challenge during spray drying because of high viscosity; it clogged the 1 mm nozzle of the spray dryer frequently. The operation was stopped to clean the nozzle of the spray dryer, and it was not feasible to spray-dry this solution continuously. So, this solution with a 60:40 ratio of chitosan–EDTA disodium was not spray-dried for all three drying temperatures. Table 2 shows that only six trials were conducted for two ratio solutions.

Evaluation and characterization

Percentage yield

The percentage yield was calculated based on the total recoverable and original weight used [15].

Particle size and morphological evaluation

The surface morphology and topography of the particles were observed by the scanning electron microscope (ZEISS Sigma 360, Germany) at 20 kV (EHT) [16]. The samples were fixed on the SEM stub and coated with a thin layer of gold. Various images were taken at different magnifications. ImageJ (NIH) software was used to determine particle size by analyzing SEM images. The average Feret's diameter was reported.

Zeta potential

100 mg of CHEM prepared by both techniques were taken and constantly stirred in 10 ml triple distilled water. The resulting suspension was centrifuged for 10 min at around 5000 rpm to separate the undissolved particles. Further, this mixture was analyzed for zeta potential in Zetasizer Nano ZS (at wavelength 638 nm) with a scattering angle of 90° at 25 °C. The study was performed in triplicate (Malvern Panalytical, UK) [17].

Table 3 Least squares fit effect summary

SE-CHEM			**SD-CHEM**		
Source	**LogWorth**	***P* value**	**Source**	**LogWorth**	***P* value**
CH(1, 3)	3.703	0.0002	CH × DT	2.207	0.0062
DT(1, 3)	1.645	0.0226	CH	1.807	0.0155
CH × DT	1.332	0.0465	DT(1,3)	1.614	0.0243
Response	R^2	R^2 **Adj**	**RMSE**	**MR**	**Observation**
Summary of fit (SE-CHEM)					
Y	0.956	0.9298	1.443	89.188	9
ZP	0.825	0.7207	1.568	3.553	9
PS	0.939	0.9025	2.415	11.735	9
Summary of fit (SD-CHEM)					
Y	0.992	0.981	1.704	37.07	6
ZP	0.913	0.783	1.476	0.62	6
PS	0.956	0.892	0.348	3.85	6
Response	**Source**	**DF**	**SS**	**MS**	***F* Ratio**
Analysis of variance (SE-CHEM)					
Y	Model	3	227.42	75.81	36.36
	Error	5	10.42	2.08	**Prob > F**
	C. Total	8	237.84		0.0008*
ZP	Model	3	58.15	19.38	7.88
	Error	5	12.29	2.45	**Prob > F**
	C. Total	8	70.45		0.0243*
PS	Model	3	450.02	150.009	25.7
	Error	5	29.18	5.837	**Prob > F**
	C. Total	8	479.21		0.0018*
Analysis of variance (SD-CHEM)					
Y	Model	3	760.41	253.46	87.22
	Error	2	5.81	2.91	**Prob > F**
	C. Total	5	766.21		0.0114*
ZP	Model	3	46.01	15.33	7.03
	Error	2	4.35	2.17	**Prob > F**
	C. Total	5	50.36		0.127
PS	Model	3	5.38	1.79	14.79
	Error	2	0.24	0.12	**Prob > F**
	C. Total	5	5.62		0.064
Response	**Term**	**Estimate**	**SE**	***t* Ratio**	**Prob > |*t*|**
Parameter estimates (SE-CHEM)					
Y	Intercept	89.18	0.48	185.32	< 0.0001*
	CH(1,3)	5.71	0.58	9.7	0.0002*
	DT(1,3)	1.91	0.58	3.25	0.0227*
	CH × DT	− 1.52	0.72	− 2.11	0.0883
ZP	Intercept	3.55	0.52	6.8	0.0010*
	CH(1,3)	3.11	0.64	4.85	0.0047*
	DT(1,3)	0.19	0.64	0.3	0.7758
	CH × DT	− 0.06	0.78	− 0.09	0.9335

Table 3 (continued)

Response	Term	Estimate	SE	*t* Ratio	Prob > |*t*|
PS	Intercept	11.73	0.8	14.57	< 0.0001*
	CH(1,3)	− 7.62	0.98	− 7.73	0.0006*
	DT(1,3)	− 3.18	0.98	− 3.23	0.0233*
	CH × DT	3.17	1.2	2.63	0.0466*
Parameter estimates (SD-CHEM)					
Y	Intercept	37.07	0.69	53.27	0.0004*
	CH	5.51	0.69	7.91	0.0156*
	DT(1,3)	− 5.36	0.85	− 6.29	0.0243*
	CH × DT	− 10.76	0.85	− 12.63	0.0062*
ZP	Intercept	0.62	0.61	1.03	0.4118
	CH	2.12	0.61	3.53	0.0718
	DT(1,3)	0.75	0.73	1.02	0.4152
	CH × DT	− 2.03	0.73	− 2.76	0.11
PS	Intercept	3.85	0.14	27.13	0.0014*
	CH	− 0.86	0.14	− 6.07	0.0261*
	DT(1,3)	− 0.23	0.17	− 1.35	0.3099
	CH × DT	0.41	0.17	2.4	0.1382

* It indicates that the p value is significant. The model is significant

DF-Degree of freedom, MR-mean of response, MS-mean of squares, PS-particle size, RMSE-root mean square error, SS-sum of squares, Y-percentage yield, ZP-zeta potential

FTIR analysis

After drying the prepared samples (SD-CHEM, SE-CHEM, CH and EDTA) under vacuum, these were mixed and triturated with KBr (1:100 ratio) to form a fine mixture. This fine mixture was pressed to form the pellets in the KBr press. After placing these pellets in a sample cell, FTIR-ATR analysis was performed (FTIR PerkinElmer spectrum two, USA) in the 500–4000 cm^{-1} spectral range at ambient temperature [18].

DSC analysis

The 5–15 mg samples of SD-CHEM (Y1), SE-CHEM (C2), CH and EDTA were sealed hermetically in aluminum pans. After placing these pans on the sample pan holder and empty pans on reference pan holders in a Differential scanning calorimeter (DSC-25 TA, USA), the thermograms for each sample were recorded from a 40–400 °C temperature range with 10 °C per minute heating rate in a nitrogen atmosphere.

XRD analysis

After grinding each sample (SD-CHEM, SE-CHEM, CH and EDTA) in mortar and pestle, the formed powder was placed and pressed in a sample holder to form a compact powder and X-ray diffraction patterns of the samples were measured using the X-ray diffractometer (XRD Aeris, Malvern Panalytical, UK) at a voltage of 45 kV (with increment size of 0.03° and 0.1 as an increment time).

Flow properties

For all the batches of microparticles, the angle of repose was calculated. In it, graph paper was positioned on a flat horizontal surface, and a funnel was clamped above it with a distance between the paper and the funnel top (about 7–8 cm). 2 g of powder samples for each trial of SE-CHEM and SD-CHEM were weighed and poured into the funnel until the top of the cone-shaped only met the funnel's top. The height (h) and diameter of the cone-shaped heap of powder (D) were measured, and the angle of repose was calculated with a standard formula ($\tan \alpha = 2$ h/D). The flow is said to be excellent when the angle of repose is less than 25 degrees; on the other hand, the flow is said to be poor when the angle of repose is greater than 40 degrees. For bulk density, 2 g powder was weighed and carefully leveled without tapping into a graduated glass cylinder. To the closest graduated device, the apparent volume before tapping was read as untapped volume (USP method). This volume was used in the standard formula (Bulk density = Weight/untapped volume), and values were calculated. The volume of the powder-filled cylinder was measured after 500 tappings. The tapping was kept running until the frequency difference between the two sets of tapping was less than 0.2 percent. The final volume was noted, and the tapped density in g/ml was calculated using the standard formula (Tapped density = Weight/tapped volume). These readings were used to calculate Carr's index (CI) and

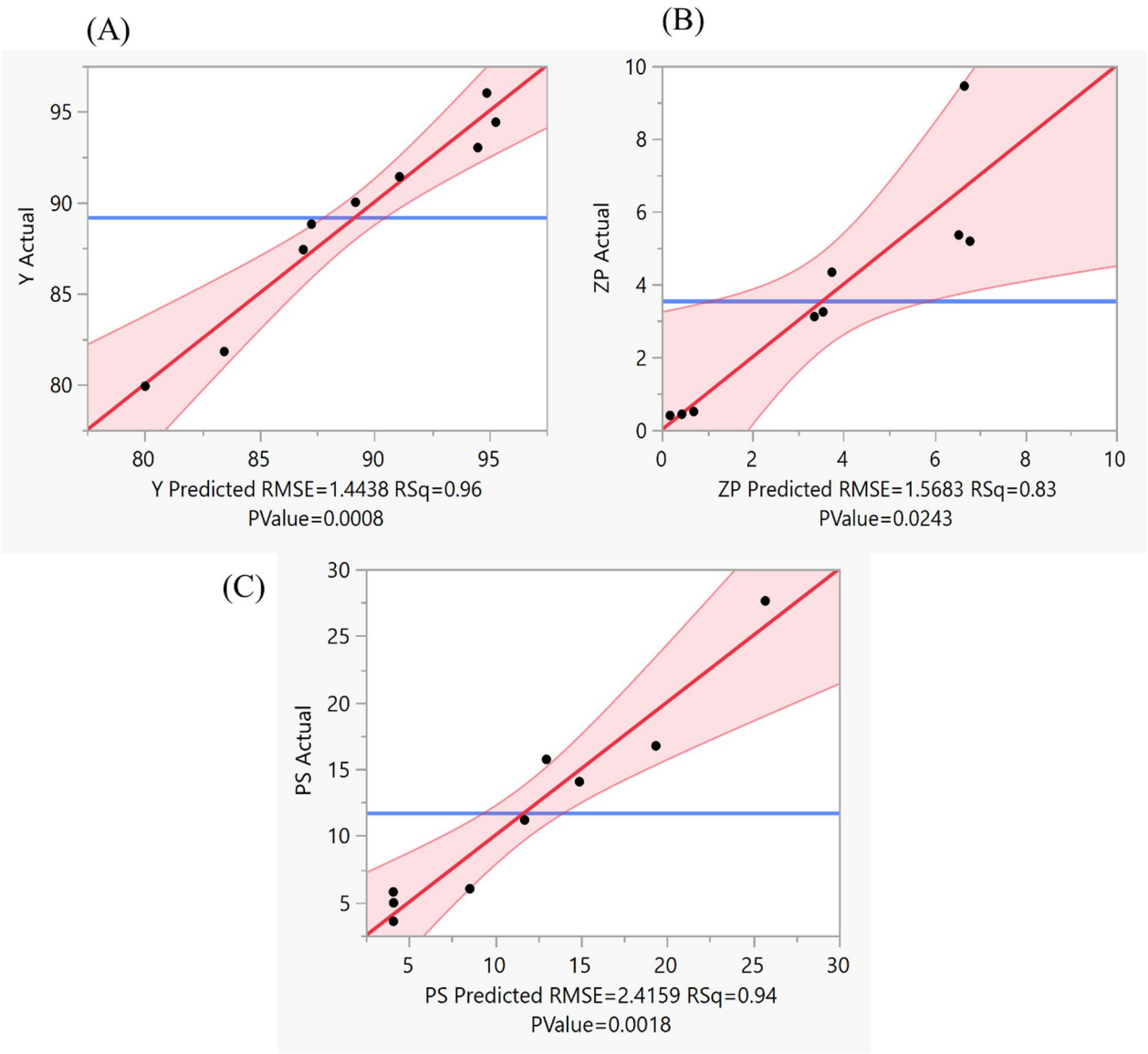

Fig. 1 Actual vs predicted plot of SE-CHEM for the responses **A** practical yield *Y*, **B** zeta potential ZP and **C** particle size PS. After 3^2 full factorial design was applied and model was run. In all the Actual vs predicted plots both actual and predicted values are quite close to each other. Here, the low RMSE (Root Mean Square Error) values in Y, ZP and PS plots indicated the model is significant and fits the data well. The *R* Squared (R^2) values in Y, ZP and PS plots predicts the percentage of the relationship between independent variables [CH (chitosan–EDTA ratio) and DT (Drying temp.)] and dependent variables (Y, ZP and PS). These plots depicted 96%, 83% and 94% relationship between the independent variables and Y, ZP and PS, respectively. *P* value less than 0.05 showed all the model is statistically significant for Y, ZP and PS

Hausner's ratio (HR). {CI = [(Tapped density – Bulk density/Tapped density) × 100] and HR = Tapped density/Bulk density}. A Carr's index of more than 25 indicates bad flowability, while if its value is less than 15, it indicates good flowability. Hausner's ratios below 1.25 suggest greater flow properties than those above 1.25 [19].

Oil adsorbing capacity (OAC) and oil desorbing capacity (ODC)

The optimized formulations of SD-CHEM and SE-CHEM, i.e., Y_1 and C_2, respectively, were taken for OAC and ODC study. The ethanolic solutions of Cremophor RH 40 and Labrafac were prepared and mixed with the

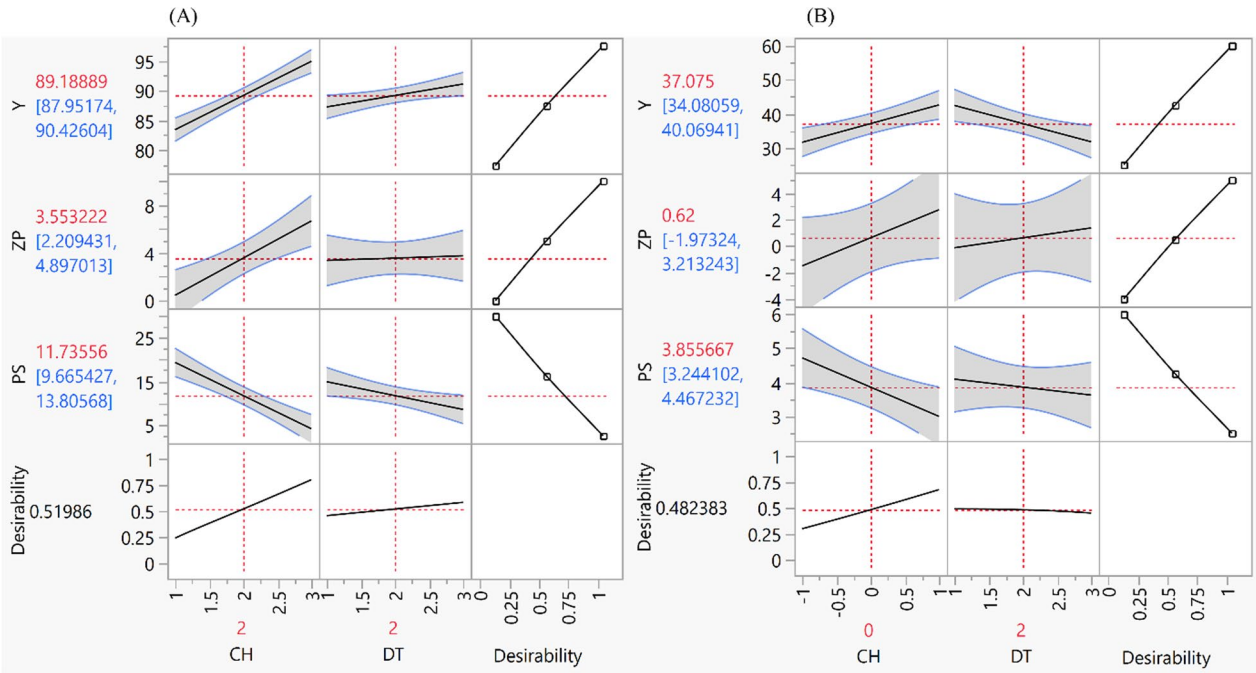

Fig. 2 Prediction profiler of practical yield (Y), zeta potential (ZP) and particle size (PS): **A** SE-CHEM, **B** SD-CHEM. The prediction profiler depicted CH (CH/EDTA ratio) as the most important independent variable, followed by DT (Drying temp.), for any change in responses of Y, ZP and PS (in both SE-CHEM and SD-CHEM). For **A** SE-CHEM, it showed that CH and DT had a positive (or additive) effect on a percentage yield (Y) and zeta potential ZP. CH and DT had a negative effect on PS. For **B** SE-CHEM, prediction profiler showed that CH and DT had a positive (or additive) effect on a percentage yield (Y) and zeta potential ZP. CH and DT had a negative effect on PS. With the use of prediction profiler, the variables value can be predicted as per needed desirability by dragging the function handles left or right in JMP

microparticles (CHEM). These mixtures were gently heated at 40 ± 4 °C to evaporate the ethanol. The pure weight of adsorbent microparticles (W_a) and the dry weight of oil-adsorbed microparticles after the complete removal of ethanol (W_b) were taken to calculate the OAC. Only those dried mixtures which showed no significant change in physical properties from the pure CHEM and were non-sticky, non-greasy and free-flowing and were considered for the OAC calculations with the following formula [5].

$$\mathrm{OAC} = \frac{W\mathrm{b} - W\mathrm{a}}{W\mathrm{a}} * 100 \quad (1)$$

The dried oil-adsorbed microparticles (W_b) were suspended in 10 ml water and gently stirred and stabilized for 1 h. This mixture was centrifuged at 3000 rpm for 10 min. The suspended particles were recovered, dried and weighed (W_c). The following formula was used for ODC [5].

$$\mathrm{ODC} = \frac{W\mathrm{b} - Wc}{Wc} * 100 \quad (2)$$

Dynamic advancing contact angle analysis and surface free energy components analysis

The advanced method was used based on the capillary rise and thin column wicking methods to find the surface free energy components of powdered solids developed by Chibowski and Perea-Carpio [21] for SD-CHEM (Y_1) and SE-CHEM (C_2) [20, 21]. The dynamic advancing contact angle and surface free energy components were determined before and after oil adsorption for microparticles. The four probe liquids with known surface tension components were used. Out of these, diiodomethane ($\gamma_l^{lw} = 50.8$, $\gamma_l^{+} = 0$, $\gamma_l^{-} = 0$) and n-hexane ($\gamma_l^{lw} = 18.4$, $\gamma_l^{+} = 0$, $\gamma_l^{-} = 0$) were apolar with known liquid apolar surface free energy component. The other two liquids, dimethyl sulphoxide (DMSO $\gamma_l^{lw} = 36$, $\gamma_l^{+} = 0.5$, $\gamma_l^{-} = 32$) and water ($\gamma_l^{lw} = 21.8$, $\gamma_l^{+} = 25.5$, $\gamma_l^{-} = 25.5$), were polar with known liquid surface free energy polar components.

In this method, 0.2 g of the samples were weighed out in the plastic tips (2 ml, Merck) with outlets blocked by nylon swabs to prevent leakage of the solid powder. The tip was tapped ten times by hand from a height of 10 cm on the laboratory table for uniform packing. The tip was

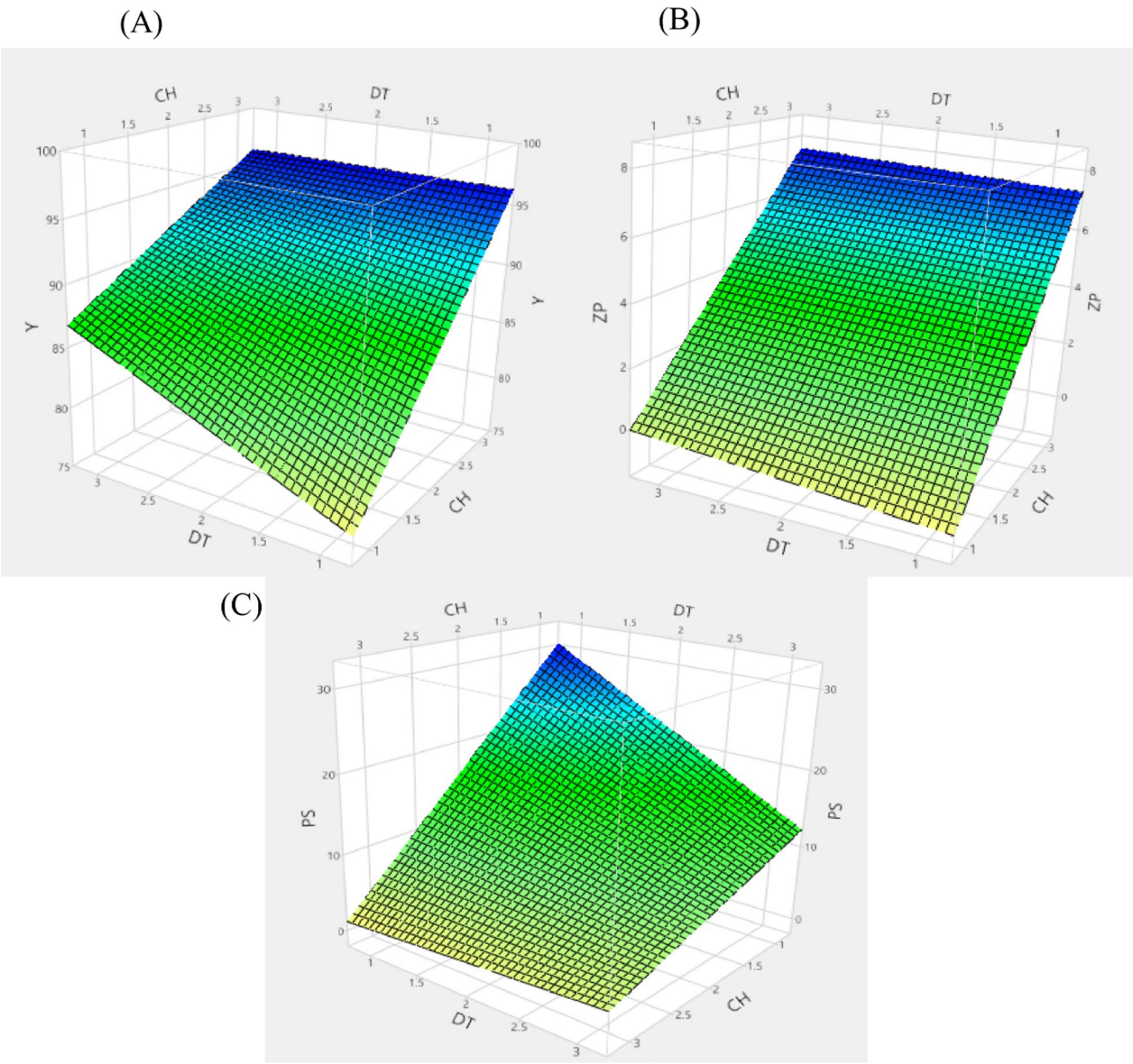

Fig. 3 Response surface diagrams of SE-CHEM in relation to CH versus DT **A** practical yield Y, **B** zeta potential ZP and **C** particle size PS. It is clear from figure **A** and **B** that a high percentage of CH (CH/EDTA ratio) from (40:60) to (60:40) leads to an increase in Y, which means when chitosan increases in (CH/EDTA ratio), then Y got increased. Similarly, when DT (Drying temp.) increased, there was an increase in both Y and ZP, which means a high drying temp was responsible for it. In the case of **C**, particle size PS, an increase in CH × DT negatively affects PS (decrease in size)

then dipped 3–4 mm into the probe liquid container (advancing manner). The tip was weighed for liquid retained by the solid powder (m_a). After that, some drops from the same probe fluid were put onto the bed powder top. The liquid was allowed to filter (receding manner), and the new weight was measured (m_r). The process was repeated three times, and the average of three determinations was used. The powdered samples (Y_1, C_2) underwent a similar procedure before and after oil adsorption for all the probe liquids.

The effective pore radius ($R_{ef.}$) was calculated by using the (m_r) of n-hexane probe liquid (surface tension, $\gamma_l = 18.4$mN/m) and acceleration due to gravity (g) in the following equation.

$$W = m_r g = 2\pi R_{ef.} \gamma_l \quad (3)$$

W = weight of the liquid in the column.

The n-hexane determines the effective radius because alkanes completely wet the solid surface. In the following equation, the effective pore radius ($R_{ef.}$), along with (m_a)

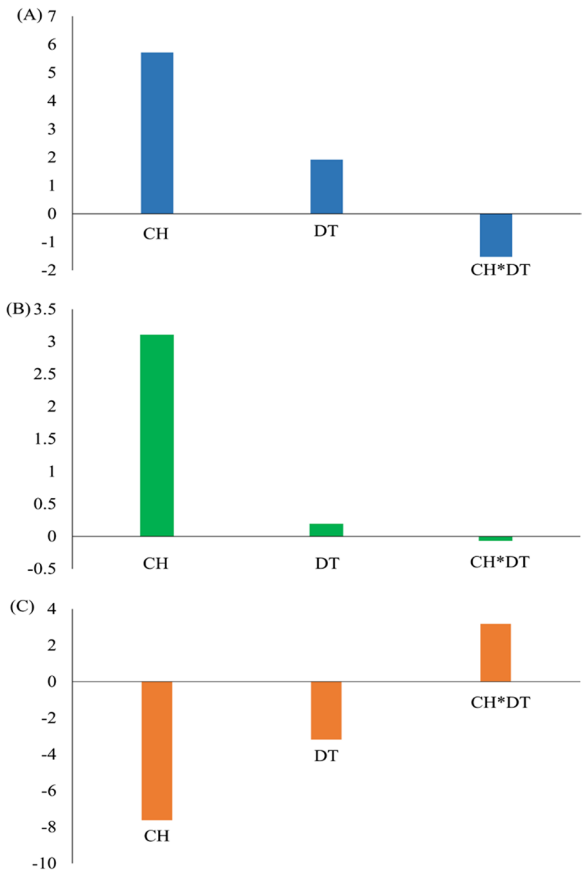

Fig. 4 Pareto charts for SE-CHEM **A** practical yield, **B** zeta potential and **C** particle size. ZP show that both CH and DT have a positive effect on it. It is clear from parameter estimates that the CH × DT interaction significantly contributes to the regression model for smaller particle size (PS). CH and DT have a negative effect on PS

of water probe liquid, was used for further calculation of the dynamic advancing contact angle (θ_a).

$$1 + \cos\theta a = \frac{m_a g}{2\pi R_{ef.}\gamma_l} \tag{4}$$

$$W_a = \gamma_l(1 + \cos\theta_a) \tag{5}$$

where $g = 9.8$ m/s^2, $\gamma_l = 72.8$ mN/m.

The advancing contact angle here remains different from the contact angle on a smooth surface of a similar solid. Hence, it cannot be used directly in the Young formula for calculating surface free energy components. The three works of adhesion (W_a) values of the used probe liquid onto the solid surface were calculated by finding out the θ_a of three probe liquids, diiodomethane, DMSO and water (by putting ma values simultaneously in Eq. 4).

Further, by putting these different W_a values simultaneously in Eq. 6 of three probe liquids (with known liquid surface free energy components, i.e., γ_l^{LW}, γ_l^{+}, γ_l^{-}), the different unknown components (γ_s^{LW} apolar Lifshitz–van der Waals, γ_s^{-} electron donor and γ_s^{+} electron acceptor interactions) can be solved.

$$W_a = 2\left[\left(\gamma_s^{LW}\gamma_l^{LW}\right)^{1/2} + \left(\gamma_s^{+}\gamma_l^{-}\right)^{1/2} + \left(\gamma_s^{-}\gamma_l^{+}\right)^{1/2}\right] \tag{6}$$

Results

The process was optimized using a factorial experimental design (3^2), the chitosan–EDTA disodium ratio and processing temperature varied on three levels. The disodium salt was used to increase the solubility of the EDTA, as it remains insoluble in the acidic pH. The dropwise addition of the EDTA disodium into the chitosan–acetic acid mixture ensures no precipitation of the solution, which is otherwise observed.

In Tables 1 and 2, all the results of percentage yield (%), zeta potential (mV) and particle size (μm) are given for both SE-CHEM and SD-CHEM.

Optimization

Optimization of Solvent evaporation method by QbD

As per the mentioned method, SE-CHEM were synthesized and analyzed for the response for Y (percentage yield %), ZP (zeta potential mV) and PS (particle size μm). The independent variables CH (CH/EDTA ratio) and DT (drying temp.) were given three levels (1, 2 and 3), as mentioned in Table 1. All nine experiment runs and analyzed responses were put in the least squares fit regression analysis using JMP 16 (Trial).

In the effect summary in Table 3, LogWorth and p value for CH, DT and CH × DT are mentioned for SE-CHEM, which indicates CH as the essential variable in this model, followed by DT and CH × DT (interaction). Actual vs. predicted plots are given in Fig. 1 for all the responses, showing that both actual and predicted values are quite close. Table 3, for a summary of fit, indicates that the R^2 values are closer to one, signifying a good model fit. In Table 3, ANOVA results are summarized, which shows the models are significant (p values less than 0.05) for all the responses.

Table 3 (for parameter estimates) and Fig. 2a for prediction profiler depict CH (CH/EDTA ratio) as the most important independent variable, followed by DT, for any change in responses. The small particle size of the adsorbent base powder is essential for a high surface area to have high oil adsorption and desorption. It shows that CH and DT have a positive (or additive) effect on a percentage yield (Y%). The parameter estimates and prediction profiler in Fig. 2a for ZP show that both CH and DT have a positive effect on it. It is clear from parameter

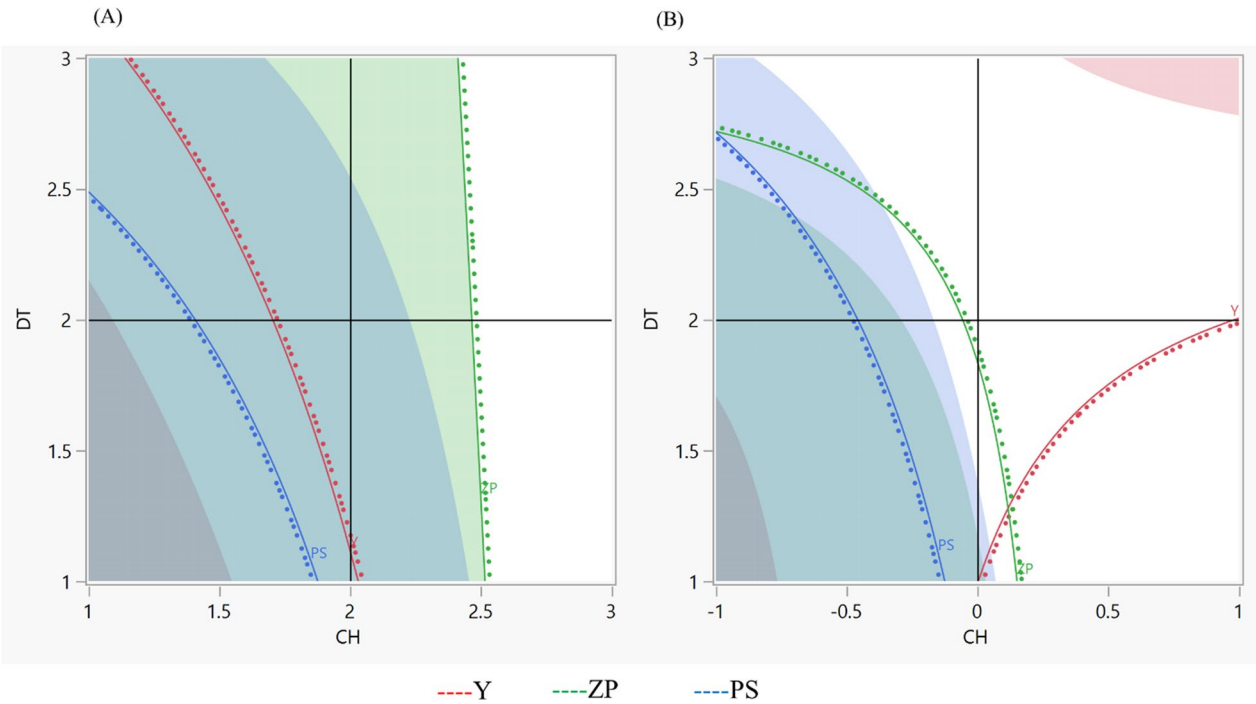

Fig. 5 Contour plots of practical yield (Y), zeta potential (ZP) and particle size (PS): **A** SE-CHEM, **B** SD-CHEM. **A** In this contour plot, white area shows the design space where the Y and ZP will be maximum and PS will be minimum. So, the desirability for percentage yield (%) and zeta potential (mV) is always more than 84%, 8 mV and for particle size (μm) < 6 μm can be obtained with CH/EDTA ratio (60:40) and drying temperature (70 °C). **B** The white area of contour plot, shows the design space where the Y and ZP will be maximum and PS will be minimum. So, from these optimization studies, the desirability for percentage yield (%) and zeta potential (mV) are always more than 55%, 4 mV and for particle size (μm) < 3 μm can be obtained with CH/EDTA ratio (50:50) and drying temperature (110 °C)

estimates that the CH × DT interaction significantly contributes to the regression model for smaller particle size (PS). CH and DT have a negative effect on PS. The response surface diagrams (Fig. 3) and Pareto charts (Fig. 4) confirm the same results. Pareto charts also show the individual effect of each independent variable and their interaction on both responses. The fitted equations for all the responses are:

For percentage yield (Y):

$$89.188 + 5.716 \times (:\mathrm{CH} - 2) + 1.916 \times (:\mathrm{DT} - 2) + (:\mathrm{CH} - 2) \times (:\mathrm{DT} - 2) \times -1.525$$

For zeta potential (ZP):

$$3.553 + 3.106 \times (:\mathrm{CH} - 2) + 0.1925 \times (:\mathrm{DT} - 2) + (:\mathrm{CH} - 2) \times (:\mathrm{DT} - 2) \times 0.068$$

For particle size (PS):

$$11.735 + -7.625 \times (:\mathrm{CH} - 2) + -3.183 \times (:\mathrm{DT} - 2) + (:\mathrm{CH} - 2) \times (:\mathrm{DT} - 2) \times 3.17625$$

The optimization of the selected responses was targeted with a desirability function. For this purpose, Y and ZP were maximized, and PS was minimized. In Fig. 5a (contour plot), the white area shows the design space where the Y and ZP will be maximum and PS will be minimum.

So, from these optimization studies, the desirability for percentage yield (%) and zeta potential (mV) is always more than 84%, 8 mV and for particle size (μm) < 6 μm can be obtained with CH/EDTA ratio (60:40) and drying temperature (70 °C). So, the C_2 formulation in Table 1 is the optimized formulation with maximum desirability.

Optimization of spray drying method by QbD

The SD-CHEM were synthesized and analyzed for the response for Y (percentage yield %), ZP (zeta potential mV) and PS (particle size, μm). The independent variables CH (CH/EDTA ratio) with two levels (− 1 and 1) and DT (drying temp.) were given three levels (1, 2 and 3), as mentioned in Table 2. All six experiment runs and analyzed responses were put in the least squares fit regression analysis using JMP 16 (Trial).

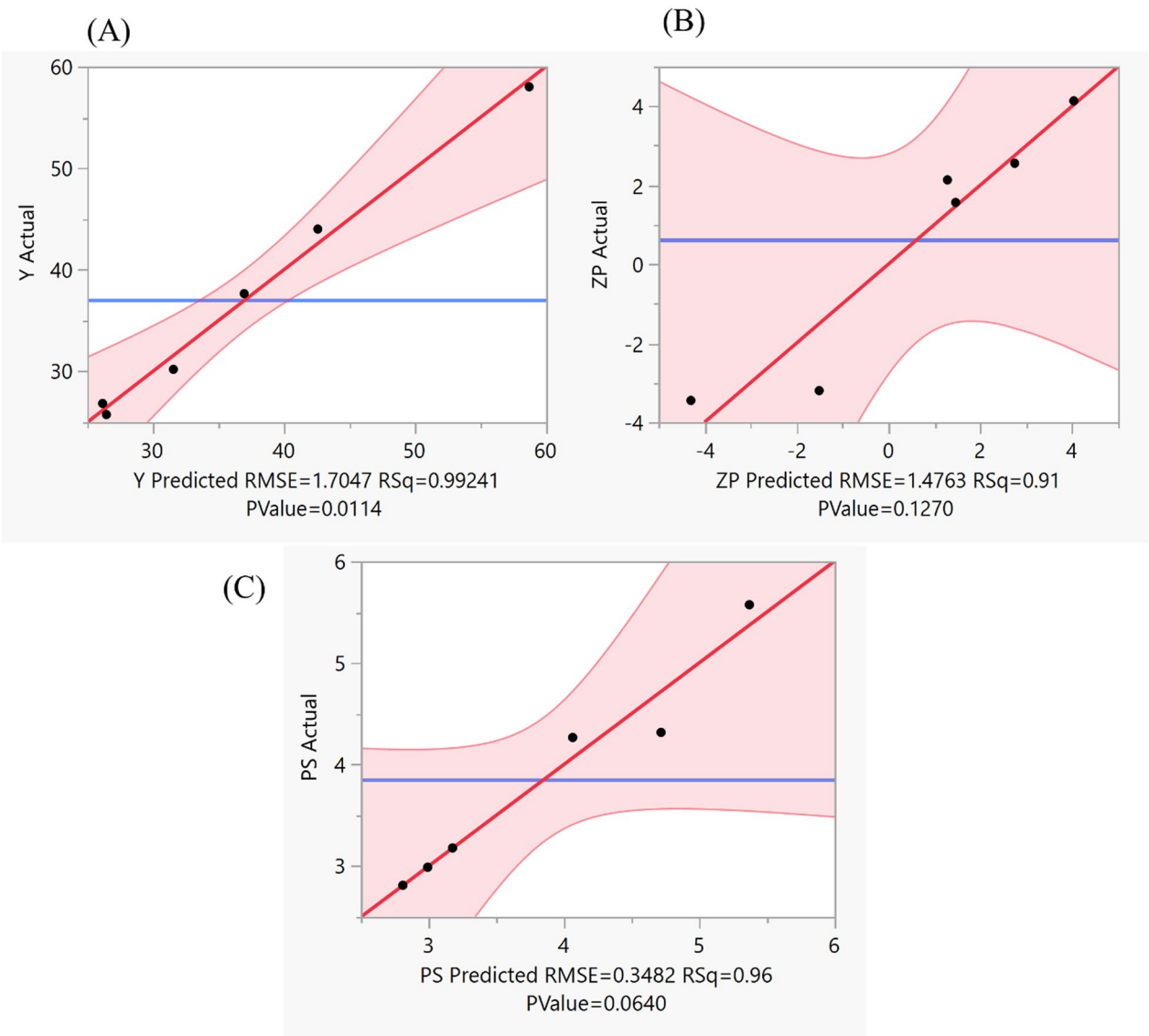

Fig. 6 Actual versus predicted plot of SD-CHEM for the responses **A** practical yield Y, **B** zeta potential ZP and **C** particle size PS. After 3^2 full factorial design was applied and model was run. In all the Actual versus predicted plots both actual and predicted values are quite close to each other. Here, the low RMSE (Root Mean Square Error) values in Y, ZP and PS plots indicated the model is significant and fits the data well. The RSq (R^2) values in Y, ZP and PS plots predict the percentage of the relationship between independent variables [CH (chitosan–EDTA ratio) and DT (Drying temp.)] and dependent variables (Y, ZP and PS). These plots depicted 99%, 91% and 96% relationship between the independent variables and Y, ZP and PS, respectively. P value less than 0.05 showed the model is statistically significant for Y and ZP and *P* value 0.06 is very close to statistically significant model for PS

In the effect summary in Table 3, LogWorth and p value for CH, DT and CH × DT are mentioned for SD-CHEM, which indicates CH × DT as the most important in the model, followed by CH and DT. Actual vs. predicted plots are given in Fig. 6 for all the responses, showing that both actual and predicted values are significantly close. Table 3, for a summary of fit, shows that the R^2 value for all the responses is > 0.90, signifying a good model fit. In Table 3, ANOVA results are summarized, which shows the *p* value of Y is 0.011, showing it is a significant model. The *p* values of ZP and PS are 0.127 and 0.064, respectively, which is almost significant for PS and not for ZP.

Table 3 (for parameter estimates) and Fig. 2b for prediction profiler depict CH × DT as the model's most important contributor for Y and PS responses. CH is the most important contributor to the ZP response. It shows on Y (%), and CH has a positive effect, while DT

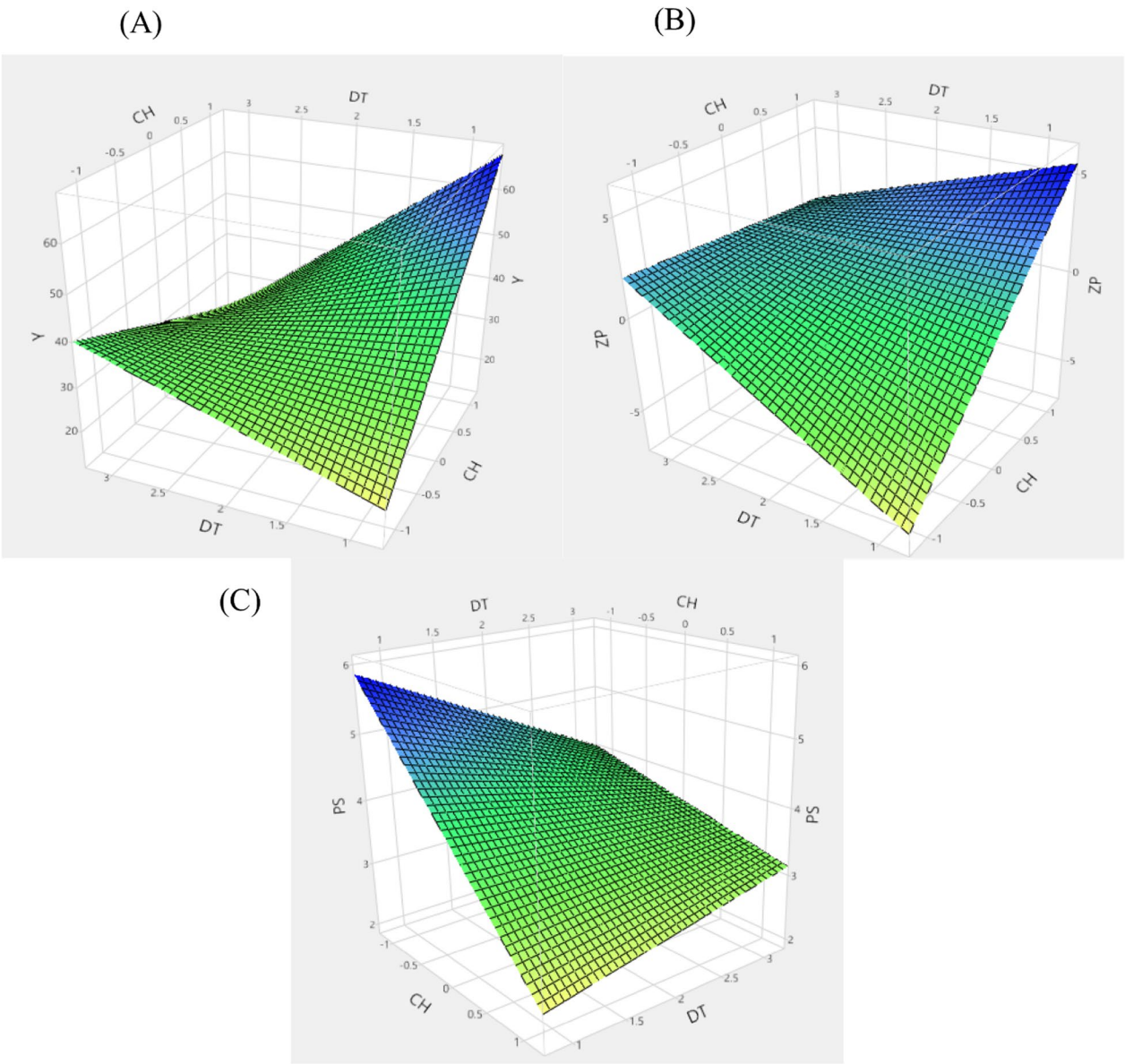

Fig. 7 Response surface diagrams of SD-CHEM in relation to CH/EDTA and DT versus **A** practical yield Y, **B** zeta potential ZP and **C** particle size PS. From figure **A** and **B** that a high percentage of CH (CH/EDTA ratio) from (40:60) to (60:40) leads to an increase in Y, which means when chitosan increases in (CH/EDTA ratio), then Y got increased. Similarly, when DT (Drying temp.) increased, there was an increase in both Y and ZP, which means a high drying temp was responsible for it. In the case of **C**, particle size PS, an increase in CH × DT negatively affects PS (decrease in size)

negatively affects it. Both CH and DT positively affect ZP and have a negative effect on PS. The response surface diagrams (Fig. 7) and Pareto charts (Fig. 8) confirm the same results. The fitted equations for the responses are as follows:

For percentage yield (Y):

$$37.075 + 5.508\times : \mathrm{CH} + -5.362 \times (: \mathrm{DT} - 2) + : \mathrm{CH} \times (: \mathrm{DT} - 2) \times -10.762$$

For zeta potential (ZP):

$$0.62 + 2.126\times : \mathrm{CH} + 0.752 \times (: \mathrm{DT} - 2) + : \mathrm{CH} \times (: \mathrm{DT} - 2) \times -2.037$$

For particle size (PS):

$$3.855 + -0.862\times : \mathrm{CH} + -0.234 \times (: \mathrm{DT} - 2) + : \mathrm{CH} \times (: \mathrm{DT} - 2) \times 0.418$$

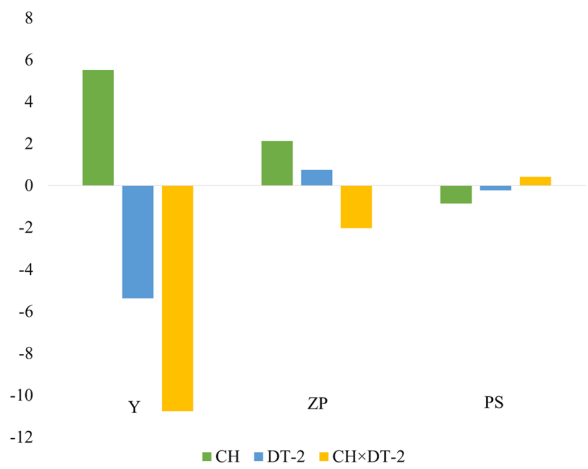

Fig. 8 Pareto charts for SD-CHEM **A** practical yield, **B** zeta potential and **C** particle size. It shows on Y (%), CH has a positive effect, while DT negatively affects it. Both CH and DT positively affect ZP and have a negative effect on PS

The optimization of the selected responses was targeted with a desirability function. For this purpose, Y and ZP were maximized, and PS was minimized. In Fig. 5b (contour plot), the white area shows the design space where the Y and ZP will be maximum and PS will be minimum.

So, from these optimization studies, the desirability for percentage yield (%) and zeta potential (mV) are always more than 55%, 4 mV and for particle size (μm) < 3 μm can be obtained with CH/EDTA ratio (50:50) and drying temperature (110 °C). So, the Y_1 formulation in Table 2 is optimized with maximum desirability.

FTIR analysis

FTIR spectra of the prepared SE-CHEM and SD-CHEM, along with chitosan and EDTA disodium, are shown in Figs. 9 and 10, respectively. Chitosan FTIR spectra showed strong absorption bands between 2967 and 2937 cm^{-1}, which correlated with C–H stretching, a characteristic of a typical polysaccharide group. The presence of residual N-acetyl groups was observed at an absorption peak of 1657 cm^{-1}, which proves that chitosan was not fully deacylated. The absorption bands 1587 cm^{-1}, 1547 cm^{-1} and 1325 cm^{-1} confirmed N–H bending of primary amine, amide II and C-N stretching of amide III respectively [22]. The absorption bands 1437 cm^{-1}, 1395 cm^{-1} and 1030 cm^{-1} corresponded to CH_2 bending, symmetrical CH_3 deformation and C–O stretching, respectively [23]. The FTIR of EDTA disodium showed N–H stretching between bands 3027–2945 cm^{-1}, C–H stretching between 2879 and 2793 cm^{-1}. The absorption bands 1666–1607 cm^{-1}, 1474 cm^{-1} and 1394 cm^{-1} showed –C=O stretching, CH_2 bending and O–H bending, respectively [24]. The optimized microparticles C_2 (SE-CHEM) and Y_1 (SD-CHEM) showed absorption bands between 1676–1657 cm^{-1} and 1693–1667 cm^{-1} respectively, representing the amide linkage. Again, the optimized microparticles C_2 (SE-CHEM) and Y_1 (SD-CHEM) showed absorption bands between 2378 and 2373 cm^{-1}, which corresponds to free acetate moieties, and indicates that all the acetate moieties were not involved in the amide linkage. Similarly, FTIR spectra of other SE-CHEMs and SD-CHEMs confirm the same results.

DSC analysis

Figure 11 shows the DSC analysis of the samples. The thermogram of chitosan, C_2 and Y_1 showed an endotherm transition near 100 °C due to the evaporation of moisture or the presence of acetic acid moieties. The exothermic transition around 311 °C corresponds to the degradation of the chitosan. The melting of the chitosan is not observable because of the amorphous regions present, so it remains near the degradation point [25]. In the EDTA thermogram, the sharp endotherm starting at 243.96 °C corresponds to the melting of it. The C_2 and Y_1 thermograms show an endothermic transition around 240 °C and exothermic transitions near 312–14 °C. This analysis confirmed the purity of the synthesized SE-CHEM and SD-CHEM.

XRD analysis

XRD patterns of the prepared SE-CHEM and SD-CHEM, along with chitosan and EDTA disodium, are shown in Figs. 12 and 13, respectively. The XRD pattern for chitosan showed two diffraction peaks, one at $2\theta = 20.37°$, which indicates the characteristic of semicrystalline regions for chitosan and the other at $2\theta = 29.57°$, which relates to calcite region [26, 27]. The EDTA disodium XRD pattern showed the major diffraction peaks at $2\theta = 21.2°$, $2\theta = 26.5°$, $2\theta = 29.8°$, $2\theta = 34.3°$ and $2\theta = 45.4°$. All these diffraction peaks correspond to the characteristic crystalline region of EDTA disodium [28]. The SD-CHEM samples showed broad diffraction peaks at $2\theta = 21.2°$, $2\theta = 23°$, $2\theta = 26.5°$ and $2\theta = 29.8°$. Similarly, SE-CHEM samples showed that diffraction peaks at $2\theta = 21.2°$ and $2\theta = 23°$ almost disappeared, and diffraction peaks at $2\theta = 26.5°$ and $2\theta = 29.8°$ were very broad and broad, respectively. These results indicate that microparticles formed from the two methods are amorphous.

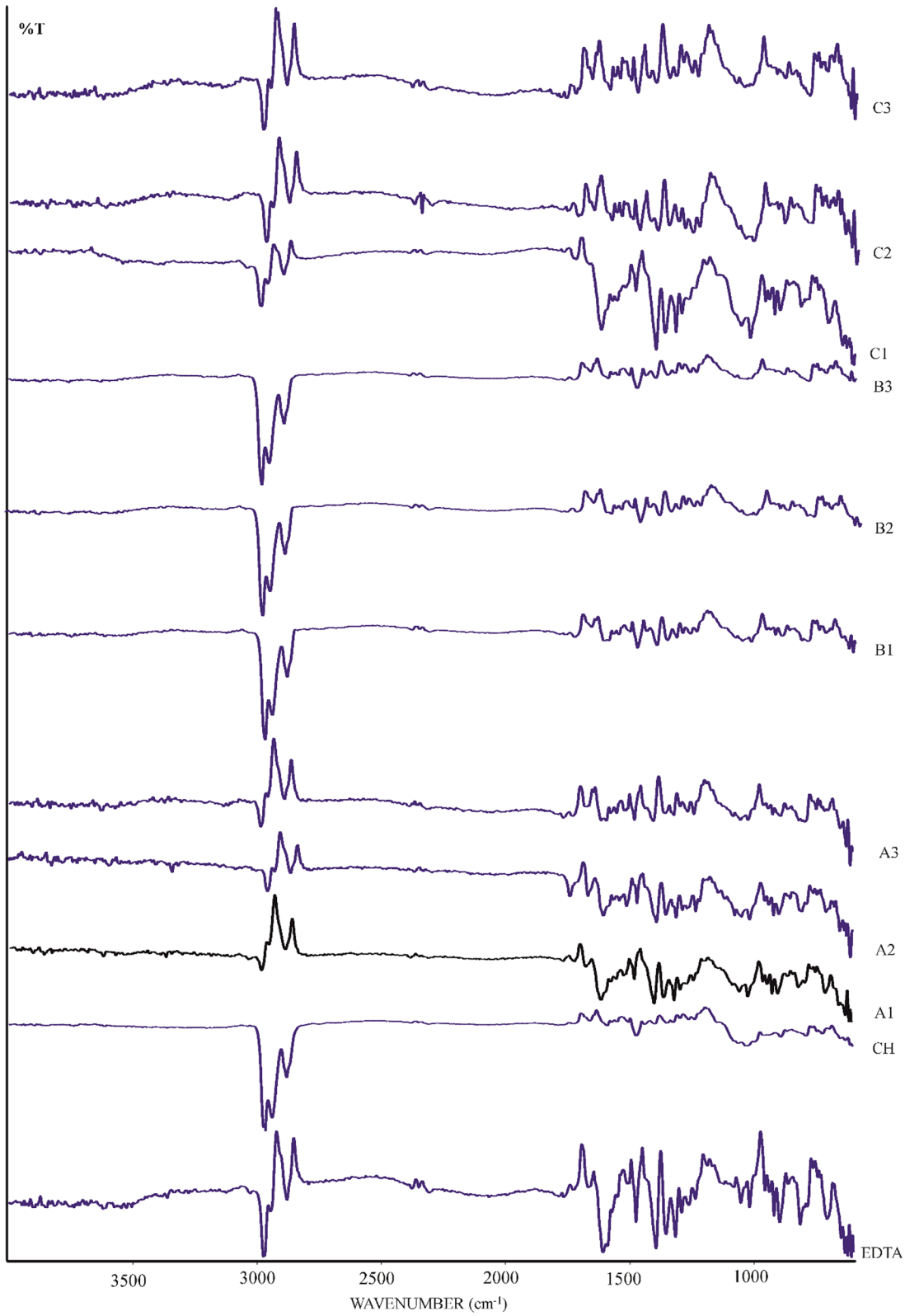

Fig. 9 FTIR spectra of chitosan (CH), EDTA disodium (EDTA) and SE-CHEM. The samples with KBr pellet were measured (at ambient temp.) for FTIR-ATR analysis in the 500–4000 cm^{-1} spectral range. The C_2 (SE-CHEM) showed absorption bands between 1676–1657 cm^{-1} and 1693–1667 cm^{-1}, representing the amide linkage. The absorption bands between 2378 and 2373 cm^{-1} correspond to free acetate moieties

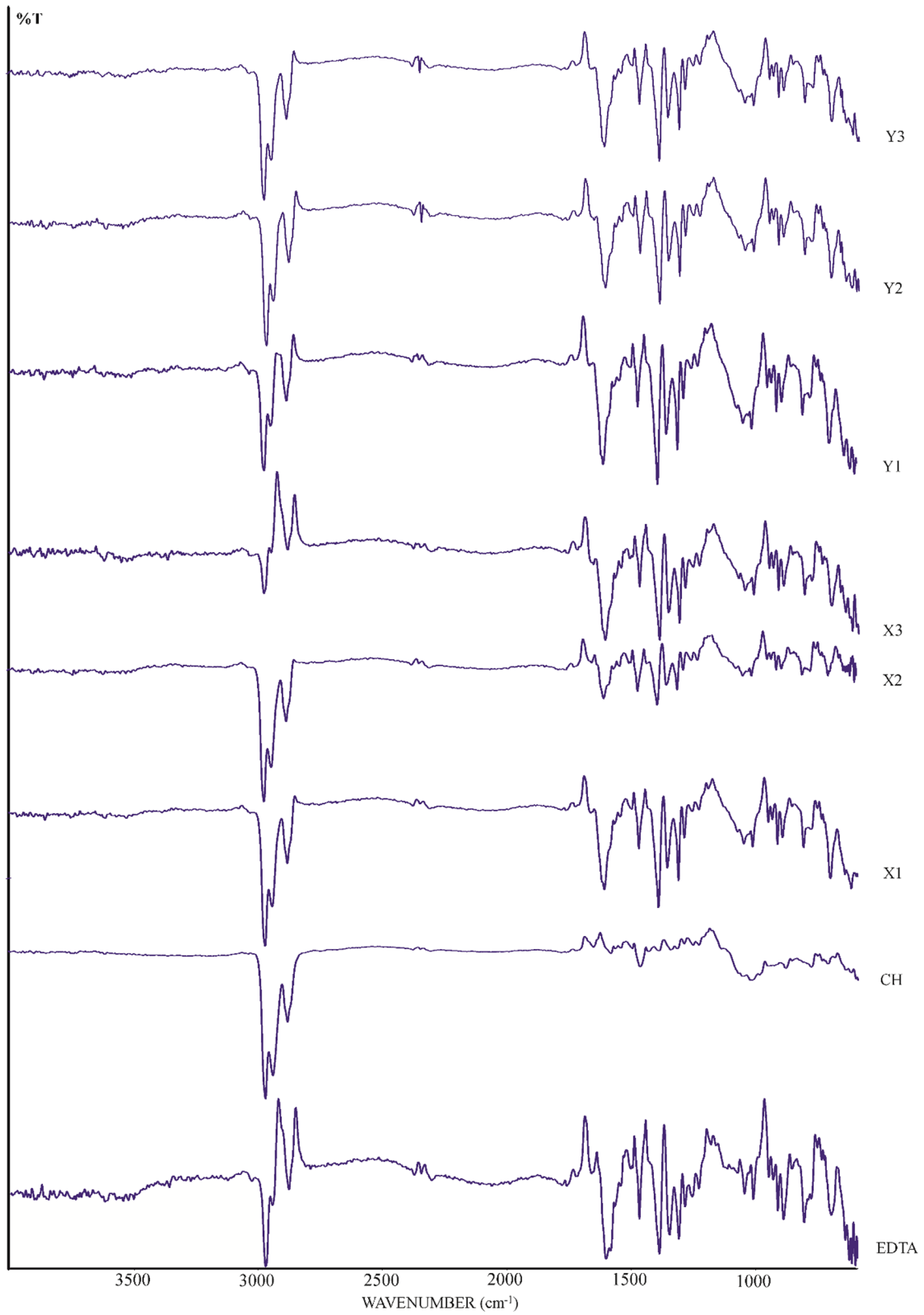

Fig. 10 FTIR spectra of chitosan (CH), EDTA disodium (EDTA) and SD-CHEM. The samples with KBr pellet were measured (at ambient temp.) for FTIR-ATR analysis in the 500–4000 cm^{-1} spectral range. The spectra of Y_1 (SD-CHEM) showed absorption bands between 1676–1657 cm^{-1} and 1693–1667 cm^{-1}, representing the amide linkage. The absorption bands between 2378 and 2373 cm^{-1} correspond to free acetate moieties

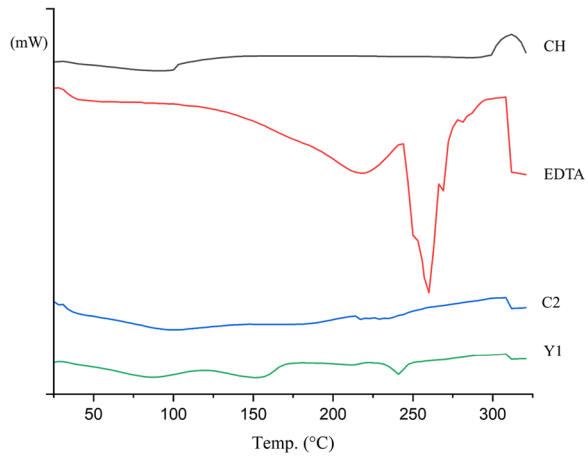

Fig. 11 DSC graphs of chitosan, EDTA disodium, C_2 and Y_1. The DSC thermograms were recorded in a Differential scanning calorimeter from 40 to 400 °C temperature range. The CH, C_2 and Y_1 showed an endotherm transition near 100 °C, 240 °C (C_2 and Y_1) and for EDTA near 243.96 °C. The CH showed exothermic transition around 311 °C and C_2 and Y_1 thermograms showed it at 312–314 °C

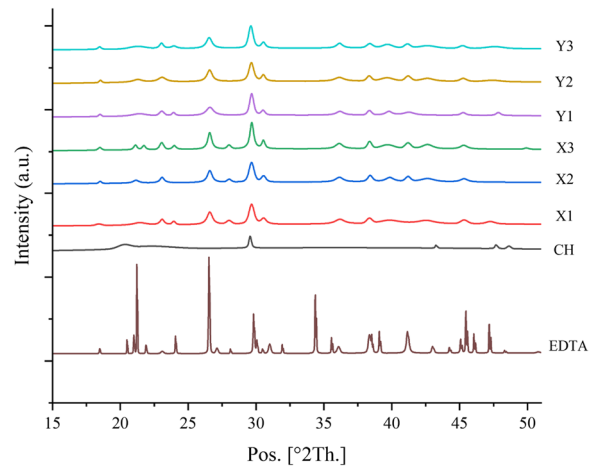

Fig. 13 XRD graphs of chitosan (CH), EDTA disodium (EDTA) and SD-CHEM samples were measured using the X-ray diffractometer at a voltage of 45 kV. The XRD pattern for chitosan showed two diffraction peaks, one at $2\theta = 20.37°$ and $2\theta = 29.57°$, while EDTA disodium diffraction peaks were at $2\theta = 21.2°$, $2\theta = 26.5°$, $2\theta = 29.8°$, $2\theta = 34.3°$ and $2\theta = 45.4°$. SD-CHEM samples showed broad diffraction peaks at $2\theta = 21.2°$, $2\theta = 23°$, $2\theta = 26.5°$ and $2\theta = 29.8°$

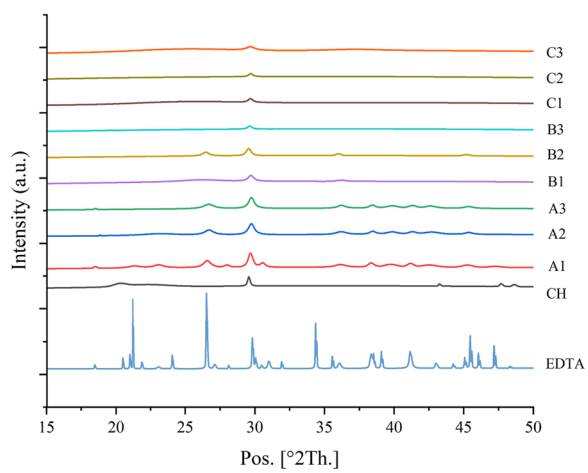

Fig. 12 XRD graphs of chitosan (CH), EDTA disodium (EDTA) and SE-CHEM samples were measured using the X-ray diffractometer at a voltage of 45 kV. The XRD pattern for chitosan showed two diffraction peaks, one at $2\theta = 20.37°$ and $2\theta = 29.57°$, while EDTA disodium diffraction peaks were at $2\theta = 21.2°$, $2\theta = 26.5°$, $2\theta = 29.8°$, $2\theta = 34.3°$ and $2\theta = 45.4°$. SE-CHEM samples showed diffraction peaks at $2\theta = 26.5°$ and $2\theta = 29.8°$

Surface characteristics

To understand the shape and surface morphology of the microparticles, the scanning electron microscope images of the chitosan, EDTA disodium, C_2 and Y_1 (shown in Fig. 14) were taken. In Fig. 14c, the SE-CHEM (C_2) microparticles had a flaky appearance with an uneven surface, providing a high surface area for the adsorption of liquid SEDDS. Figure 14d shows the SD-CHEM (Y_1) microparticles, which are much spherical with uneven surfaces and wide void spaces, leading to better oil adsorption and desorption.

Flow properties

The angle of repose (Fixed funnel method), apparent bulk density, tapped density, Carr's index and Hausner's ratio were calculated for the flowing characteristic of the microparticles, and the results are shown in Table 4, which shows all the parameters were in acceptable limits [29]. The angle of repose values for all the microparticles were between 9 and 17. Both optimized microparticles, C_2 and Y_1, were free-flowing.

OAC and ODC

Cremophor RH 40 and Labrafac were used for the OAC and ODC study; Fig. 15 shows the results. The oil adsorption for both the microparticles was significant, but Y_1 has it slightly higher than C_2 for both Labrafac and Cremophor RH 40. These results relate to the surface morphology analysis, where Y_1 showed a much spherical structure with wide voids compared to C_2, with a flaky structure.

Dynamic advancing contact angle and surface free energy components analysis

For the adsorption and desorption phenomena to happen on the microparticle's surface, the surface free energy components, i.e., apolar or dispersive component [γ^{LW}

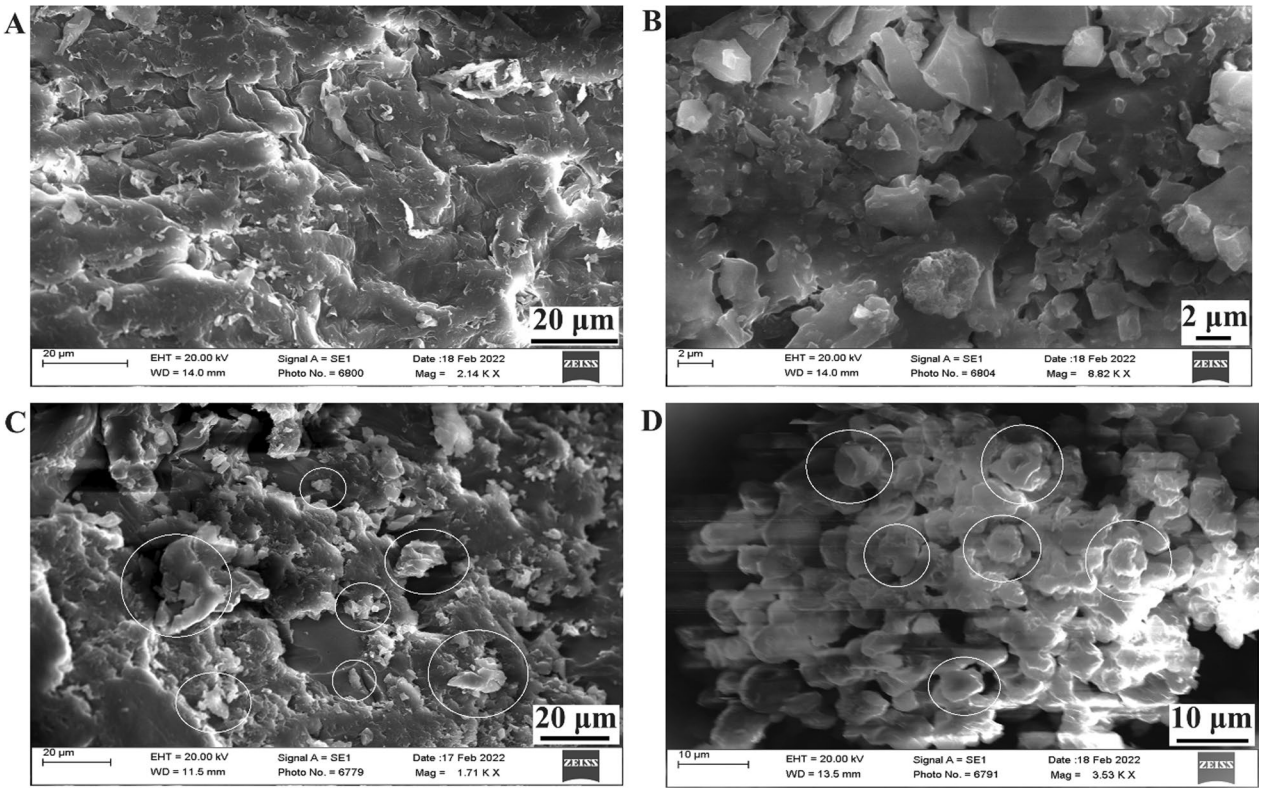

Fig. 14 Scanning electron micrographs **A** chitosan, **B** EDTA disodium, **C** C_2 and **D** Y_1. **C** The SE-CHEM (C_2) microparticles had a flaky appearance. **D** SD-CHEM (Y_1) microparticles were spherical

Table 4 Flow properties

Code	θ	ρ_b	ρ_t	CI	HR	Flowability
A_1	17 ± 1.9	0.93 ± 0.12	0.99 ± 0.23	5.72	1.06	Fair
A_2	9 ± 0.5	0.98 ± 0.19	1.12 ± 0.31	12.5	1.14	Free flow
A_3	13 ± 1.3	0.76 ± 0.36	0.8 ± 0.27	5	1.04	Free flow
B_1	12 ± 0.9	0.91 ± 0.29	1.01 ± 0.41	11.11	1.12	Free flow
B_2	16 ± 1.2	0.97 ± 0.31	1 ± 0.22	3	1.03	Fair
B_3	14 ± 1.6	1.13 ± 0.28	1.18 ± 0.39	3.89	1.04	Free flow
C_1	16 ± 0.8	0.89 ± 0.18	1.04 ± 0.47	13.5	1.15	Free flow
C_2	13 ± 1.1	0.91 ± 0.24	1.04 ± 0.29	13.12	1.15	Free flow
C_3	11 ± 0.9	0.89 ± 0.37	0.99 ± 0.41	10.5	1.11	Free flow
X_1	17 ± 0.5	0.93 ± 0.15	0.99 ± 0.36	5.72	1.06	Fair
X_2	9 ± 1.2	0.98 ± 0.45	1.12 ± 0.22	12.5	1.14	Free flow
X_3	13 ± 1.7	0.76 ± 0.26	0.8 ± 0.17	5	1.04	Free flow
Y_1	11 ± 0.6	0.9 ± 0.33	1.01 ± 0.43	11.1	1.12	Free flow
Y_2	16 ± 0.8	0.97 ± 0.18	1 ± 0.33	3	1.03	Fair
Y_3	14 ± 1.1	1.13 ± 0.22	1.18 ± 0.24	3.97	1.04	Free flow

*θ = angle of repose (°), ρ_b = bulk density (g/cm^3), ρ_t = tapped density (g/cm^3), CI = Carr's index, HR = Hausner's ratio

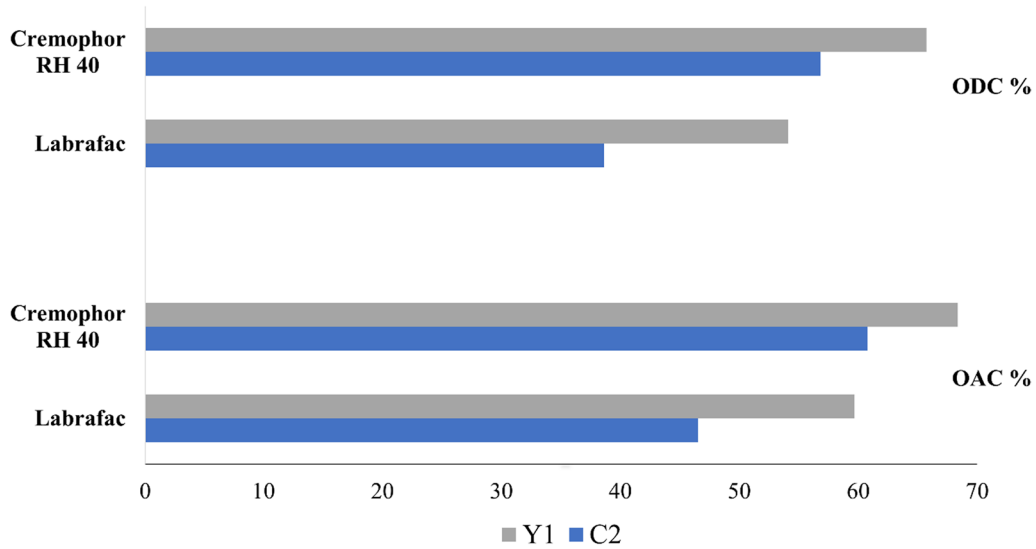

Fig. 15 Oil adsorbing capacity (OAC) and oil desorbing capacity (ODC) for C_2 and Y_1. Cremophor RH 40 and Labrafac were used for the OAC and ODC study. The OAC of Y_1 was slightly higher than C_2 for both Labrafac and Cremophor RH 40

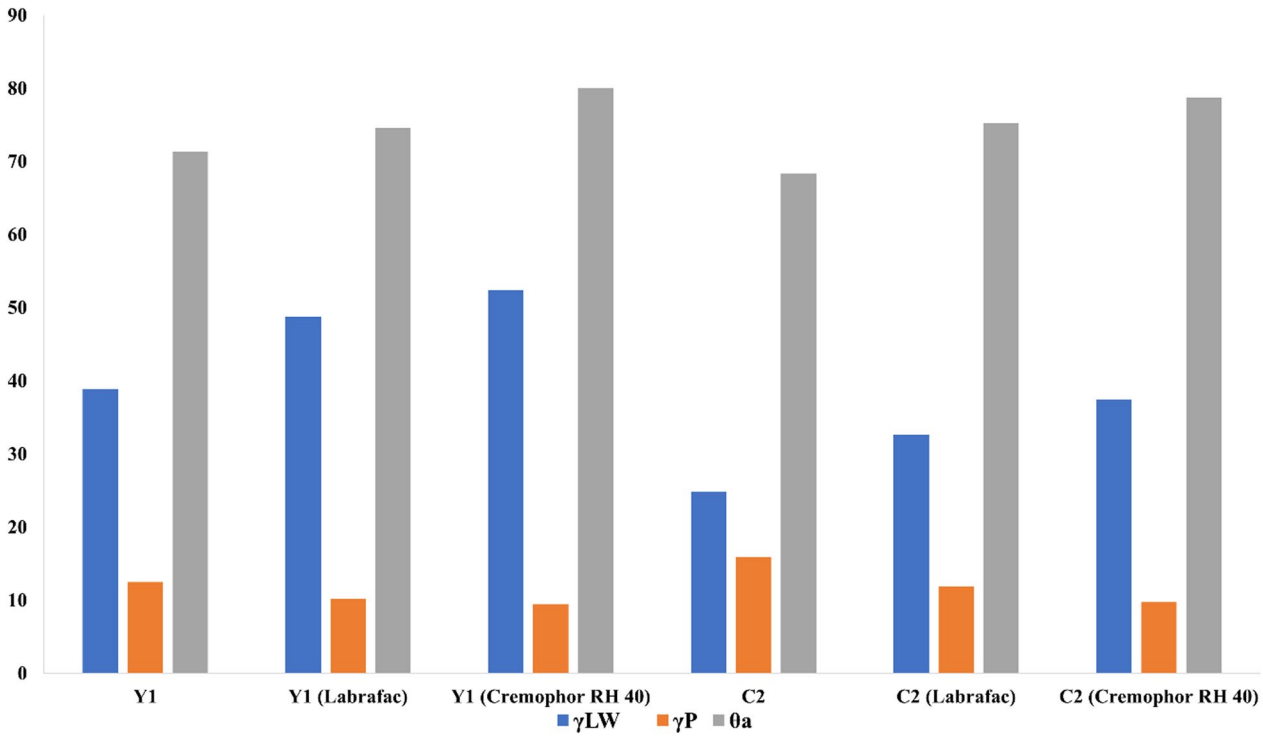

Fig. 16 Surface free energy components (dispersive component, γ^{LW} and polar component, γ^{P}) and dynamic advancing contact angles (θ_a) for C_2 and Y_1. The γ^{LW} components of C_2 and Y_1 were enhanced after oil adsorption (for both Labrafac and Cremophor RH 40). The γ^{P} components were decreased after the oil adsorptions for both microparticles. The dynamic advancing contact angles (θ_a) were also significantly increased after the oil adsorption

(mJ/m^2)] and polar component [γ^P (mJ/m^2)] are very important to understand. The γ^{LW} component is related to the hydrophobic surface, and the γ^P component relates to the hydrophilic part of the surface.

In Fig. 16, the results of the surface free energy components and dynamic advancing contact angles [θ_a (°)] are shown. The γ^{LW} components of C_2 and Y_1 were enhanced after oil adsorption (for both Labrafac and Cremophor RH 40); this indicates that increased γ^{LW} components can reduce oil droplet size significantly after reconstitution of the nanoemulsion from the surface of the adsorbent microparticles. In contrast, the γ^P components were decreased after the oil adsorptions for both microparticles. This result is significant in understanding that the microparticles can give ample surface free energy for the stable nanoemulsion, leading to good oil desorption.

The dynamic advancing contact angles (θ_a) were also significantly increased after the oil adsorption. Increased θ_a indicates the hydrophobicity of the surface, which is vital for the development of stable nanoemulsion.

Discussion

The solid adsorbent base with an excellent hydrophobic surface, oil adsorption and desorption capacities will play a crucial role in developing the S-SEDDS [30]. Hence, an attempt was made to develop the microparticles of chitosan–EDTA disodium. Such adsorbent microparticles will allow the incorporation of poorly water-soluble and thermolabile drugs into the S-SEDDS [31]. The solvent evaporation and spray drying techniques were explored to synthesize and characterize SE-CHEM and SD-CHEM microparticles, respectively. In the preliminary study, it was evident that the chitosan–EDTA disodium ratio and processing temperature in the solvent evaporation and spray drying procedures play a crucial role in the various properties of the microparticles like water solubility, yield, particle size and zeta potential. So, optimization was required for the development of the CHEM. The process was optimized using 3^2 full factorial designs, which showed a CH/EDTA ratio (60:40) and drying temp. 70 °C for solvent evaporation method and inlet temp. 110 °C and CH/EDTA ratio (50:50) produced SE-CHEM (C_2) and SD-CHEM (Y_1), respectively, with highest yield, zeta potential and lowest particle size. The different characterization studies like DSC and FTIR analysis for both optimized microparticles confirmed the amide conjugation between the CH and EDTA and free acetate moieties' existence. XRD study confirmed the broadening of the diffraction peaks for both C_2 and Y_1, suggesting the amorphous character of the particles. The high oil adsorption and desorption were achieved for both microparticles, confirmed by OAC and ODC studies. The ODC is closer to the OAC, which signifies that the amount of oil adsorbed by the microparticles will be desorbed in a very close quantity to adsorption. Surface morphology analysis through SEM images confirmed the flaky appearance of C_2 and Y_1, showing a spherical shape with voids. Flowability analysis revealed that both the microparticles were free-flowing. The surface free energy component analysis before and after oil adsorption revealed the enhancement in the dispersive components for both microparticles; this property leads to a reduction in oil droplet size on reconstitution of S-SEDDS, whereas reduced polar components after oil adsorption suggest microparticle's ability to provide sufficient surface free energy for the stability of the nanoemulsion after reconstitution. The enhanced dynamic advancing contact angles for C_2 and Y_1 indicated the hydrophobic surface of the microparticles, which was evident in high OAC for both microparticles. All these results suggest that both the microparticles can serve as stable adsorbent base for solid SEDDS to produce stable nanoemulsion after reconstitution.

Conclusion

This study has reported development of superior adsorbent carrier (microparticles) by solvent evaporation and spray drying techniques. The development of the CH-EDTA disodium microparticles (adsorbent carriers) by the solvent evaporation and spray drying methods is simplistic and practical, with the potential to be adopted at an industrial scale. The results of improved OAC, ODC and surface free energy components were satisfactory. They will prove beneficial for these microparticles to fabricate them with the liquid self-emulsifying drug delivery systems. The microparticles developed with both techniques were superior in their qualities as an adsorbent base for the solidification of SEDDS. However, if we compare both techniques, the microparticles developed by the spray drying technique were better than those from the solvent evaporation technique. The SE-CHEM had the advantage of a greater percentage yield as no minimal loss occurred during production, while SE-CHEM suffered a more significant loss and had a low percentage yield during the process. Further, the fabrication of these microparticles with SEDDS (of suitable drugs) is required to form a solid self-emulsifying drug delivery system, whose analysis in *in vitro* and *ex vivo* conditions will give a clear image of these microparticle's ability to enhance the drug loading, dissolution and bioavailability and to form a stable solid self-emulsifying drug delivery system.

Abbreviations

ANOVA	Analysis of variance
CH	Chitosan–EDTA disodium ratio
CHEM	Chitosan–EDTA disodium microparticles
DMSO	Dimethyl sulfoxide
DSC	Differential scanning calorimetry
DT	Drying temperature
EDTA	EDTA disodium
FTIR	Fourier-transform infrared spectroscopy
OAC	Oil adsorbing capacity
ODC	Oil desorbing capacity
PS	Particle size
SD-CHEM	Spray-dried-Chitosan–EDTA disodium microparticles
SE-CHEM	Solvent-evaporated-Chitosan–EDTA disodium microparticles
SEDDS	Self-emulsifying drug delivery system
SEM	Scanning electron microscope
S-SEDDS	Solid self-emulsifying drug delivery system
XRD	X-ray diffraction analysis
Y	Practical yield
ZP	Zeta potential

Acknowledgements
Not applicable.

Author contributions
MK carried out formulation and evaluation and wrote the original draft. PAC supported in FTIR, DSC and XRD analysis and interpretations. ST and SKJ supported in design of spray drying procedure and carried out it. AF and VC contributed to reviewing, editing and supervision.

Funding
None.

Availability of data and materials
Data are available on request from the authors.

Declarations

Ethical approval and consent of participate
Not applicable.

Consent for publication
Not applicable.

Competing interests
The authors declare that they have no competing interests.

Author details
[1]Department of Pharmaceutical Sciences, HNB Garhwal University, Srinagar, Garhwal, Uttarakhand, India. [2]University Institute of Pharmaceutical Sciences and Research, Baba Farid University of Health Sciences, Faridkot, Punjab, India. [3]Department of Pharmaceutical Sciences, Guru Nanak Dev University, Amritsar, Punjab, India. [4]Department of Pharmaceutical Sciences and Coordinator, Centre for Basic and Translational Research in Health Sciences, Guru Nanak Dev University, Amritsar, Punjab, India.

Received: 26 December 2023 Accepted: 29 January 2024
Published online: 12 February 2024

References

1. Seo YG, Kim D-W, Cho KH, Yousaf AM, Kim DS, Kim JH, Kim JO, Yong CS, Choi H-G (2015) Preparation and pharmaceutical evaluation of new tacrolimus-loaded solid self-emulsifying drug delivery system. Arch Pharm Res 38:223–228
2. Nikolakakis I, Partheniadis I (2017) Self-emulsifying granules and pellets: composition and formation mechanisms for instant or controlled release. Pharmaceutics 9:50
3. Bayan MF, Chandrasekaran B, Alyami MH (2023) Development and characterization of econazole topical gel. Gels 9:929
4. Sander C, Holm P (2009) Porous magnesium aluminometasilicate tablets as carrier of a cyclosporine self-emulsifying formulation. AAPS PharmSciTech 10:1388
5. Singh D, Tiwary AK, Bedi N (2019) Role of porous carriers in the biopharmaceutical performance of solid SMEDDS of canagliflozin. DDF 12:179–198
6. Zhang Y, He L, Yue S, Huang Q, Zhang Y, Yang J (2017) Characterization and evaluation of a self-microemulsifying drug delivery system containing tectorigenin, an isoflavone with low aqueous solubility and poor permeability. Drug Deliv 24:632–640
7. Nazzal S, Smalyukh II, Lavrentovich OD, Khan MA (2002) Preparation and in vitro characterization of a eutectic based semisolid self-nanoemulsified drug delivery system (SNEDDS) of ubiquinone: mechanism and progress of emulsion formation. Int J Pharm 235:247–265
8. Shao A, Chen G, Jiang N, Li Y, Zhang X, Wen L, Yang F, Wei S (2013) Development and evaluation of self-microemulsifying liquid and granule formulations of brucea javanica oil. Arch Pharm Res 36:993–1003
9. Park J-B, Choi B-K, Kang C-Y (2015) Effects of absorbent materials on a self-emulsifying drug delivery system for a poorly water soluble drug. J Pharm Investig 45:529–539
10. Singh K, Suri R, Tiwary AK, Rana V (2012) Chitosan films: crosslinking with EDTA modifies physicochemical and mechanical properties. J Mater Sci Mater Med 23:687–695
11. Cui F, Shi K, Zhang L, Tao A, Kawashima Y (2006) Biodegradable nanoparticles loaded with insulin–phospholipid complex for oral delivery: Preparation, in vitro characterization and in vivo evaluation. J Control Release 114:242–250
12. Singh SK, Vuddanda PR, Singh S, Srivastava AK (2013) A comparison between use of spray and freeze drying techniques for preparation of solid self-microemulsifying formulation of valsartan and in vitro and in vivo evaluation. Biomed Res Int 2013:1–13
13. Verma R, Kaushik D (2020) Design and optimization of candesartan loaded self-nanoemulsifying drug delivery system for improving its dissolution rate and pharmacodynamic potential. Drug Deliv 27:756–771
14. Singh K, Tiwary AK, Rana V (2013) Spray dried chitosan-EDTA superior microparticles as solid substrate for the oral delivery of amphotericin B. Int J Biol Macromol 58:310–319
15. Aldeeb RA, El-Miligi MF, El-Nabarawi M, Tag R, Amin HMS, Taha AA (2022) Enhancement of the solubility and dissolution rate of telmisartan by surface solid dispersions employing superdisintegrants, hydrophilic polymers and combined carriers. Sci Pharm 90:71
16. Shazly G, Mohsin K (2015) Dissolution improvement of solid self-emulsifying drug delivery systems of fenofi brate using an inorganic high surface adsorption material. Acta Pharm 65:29–42
17. Rathore C, Hemrajani C, Sharma AK et al (2023) Self-nanoemulsifying drug delivery system (SNEDDS) mediated improved oral bioavailability of thymoquinone: optimization, characterization, pharmacokinetic, and hepatotoxicity studies. Drug Deliv Transl Res 13:292–307
18. Blindheim FH, Ruwoldt J (2023) The effect of sample preparation techniques on lignin Fourier transform infrared spectroscopy. Polymers 15:2901
19. Dixit M, Kini AG, Kulkarni PK (2010) Preparation and characterization of microparticles of piroxicam by spray drying and spray chilling methods. Res Pharm Sci 5:89–97
20. Chibowski E, Perea-Carpio R (2001) A novel method for surface free-energy determination of powdered solids. J Colloid Interface Sci 240:473–479
21. Fukami J, Yonemochi E, Yoshihashi Y, Terada K (2006) Evaluation of rapidly disintegrating tablets containing glycine and carboxymethylcellulose. Int J Pharm 310:101–109
22. Lim S-H, Hudson SM (2004) Synthesis and antimicrobial activity of a water-soluble chitosan derivative with a fiber-reactive group. Carbohyd Res 339:313–319
23. FernandesQueiroz M, Melo K, Sabry D, Sassaki G, Rocha H (2014) Does the use of chitosan contribute to oxalate kidney stone formation? Mar Drugs 13:141–158
24. Eshraghi F, Nezamzadeh-Ejhieh A (2018) EDTA-functionalized clinoptilolite nanoparticles as an effective adsorbent for Pb(II) removal. Environ Sci Pollut Res 25:14043–14056
25. Acosta-Ferreira S, Castillo OS, Madera-Santana JT, Mendoza-García DA, Núñez-Colín CA, Grijalva-Verdugo C, Villa-Lerma AG, Morales-Vargas AT,

Rodríguez-Núñez JR (2020) Production and physicochemical characterization of chitosan for the harvesting of wild microalgae consortia. Biotechnol Rep 28:e00554
26. Manivannan M, Dhas SAMB, Balakrishnan M, Jose M (2018) Study of optical and laser damage threshold in EDTA and DTPA-doped DAST single crystals. Appl Phys B 124:166
27. Eddya M, Tbib B, EL-Hami K (2020) A comparison of chitosan properties after extraction from shrimp shells by diluted and concentrated acids. Heliyon 6:e03486
28. Gu K, Maierdan Y, Chen B (2022) Effects of ethylenediamine tetra-acetic acid (EDTA) and its disodium salt derivative (EDTA-Na) on the characteristics of magnesium oxysulfate (MOS) cement. Compos B Eng 232:109654
29. Shah RB, Tawakkul MA, Khan MA (2008) Comparative evaluation of flow for pharmaceutical powders and granules. AAPS PharmSciTech 9:250–258
30. Mandić J, ZvonarPobirk A, Vrečer F, Gašperlin M (2017) Overview of solidification techniques for self-emulsifying drug delivery systems from industrial perspective. Int J Pharm 533:335–345
31. Gupta S, Kesarla R, Omri A (2013) Formulation strategies to improve the bioavailability of poorly absorbed drugs with special emphasis on self-emulsifying systems. ISRN Pharm 2013:1–16

Publisher's Note